

# Message-passing neural networks for high-throughput polymer screening

Peter C. St. John,<sup>1</sup> Caleb Phillips<sup>2</sup>, Travis W. Kemper<sup>2</sup>, A. Nolan Wilson<sup>3</sup>, Michael F. Crowley<sup>1</sup>, Mark R. Nimlos<sup>3</sup>, Ross E. Larsen<sup>2</sup>

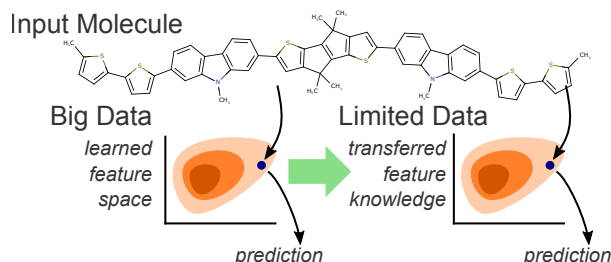
<sup>1</sup> Biosciences Center, National Renewable Energy Lab, Golden CO 80401

<sup>2</sup> Computational Sciences Center, National Renewable Energy Lab, Golden CO 80401

<sup>3</sup> National Bioenergy Center, National Renewable Energy Lab, Golden CO 80401

## Abstract

Machine learning methods have shown promise in predicting molecular properties, and given sufficient training data ML may surpass density functional theory in computational speed and chemical accuracy. However, the most accurate machine learning methods require optimized 3D molecular geometries, limiting their applicability for high-throughput screening. We show that near-optimal results for large polymeric molecules can be obtained without optimized 3D geometry, and that trained model weights can be used to improve performance on related tasks.



## Introduction

High-throughput computational screening offers the ability to explore large regions of chemical space for particular functionality, greatly enhancing the efficiency of material development efforts<sup>1-3</sup>. Due to its favorable balance between computational cost and chemical accuracy, density functional theory (DFT) has served as the workhorse of high-throughput computational material design. However, while DFT sacrifices chemical accuracy for numerical efficiency, DFT calculations are still too slow to screen the vast combinatorial landscape of potential chemical structures<sup>4</sup>. As an alternative to detailed quantum chemistry calculations, fully empirical machine learning (ML) predictions offer calculation times nearly six orders of magnitude faster than DFT ( $O(10^{-3}s)$  for ML,  $O(10^3s)$  for DFT on  $\sim 30+$  heavy atom molecules). Machine learning approaches have recently shown to be effective in reproducing DFT results given sufficient training data<sup>5</sup>, and therefore offer an opportunity to efficiently screen much larger libraries of compounds without further reduction in chemical fidelity.

Developing ML pipelines for molecular property prediction requires encoding variable-sized molecules as a finite-dimensional vector. Initial approaches used group contribution methods, molecular fingerprints, and molecular descriptors to convert molecular structures into a suitable input for dense neural networks or other ML models<sup>6-11</sup>. However, hand-engineered molecular features may not sufficiently capture all the variability present in the space of chemically feasible compounds. More recently, neural network architectures that operate directly on graph-valued inputs have been developed<sup>12</sup>, allowing ‘end-to-end’ learning on molecular space. In this approach, models simultaneously learn both how to extract appropriate features as well as how to use these features to make accurate predictions. End-to-end learning techniques have supplanted traditional methods in the fields of image recognition and computer translation, similar fields where determining a suitable numerical representation of the input data is difficult.

A number of approaches for end-to-end learning on molecules have recently been unified into a single theoretical framework, known as Message Passing Neural Networks (MPNNs)<sup>13</sup>. In MPNNs, predictions are generated from input graphs with node and edge features. The network comprises a sequence of layers, including a number of *message passing* layers and a *readout* layer. In the message passing layers, node-level state vectors are updated according to graph’s connectivity and the current states of other nodes. Following a number of message passing layers, in the readout layer a single graph-level vector is generated from all the nodes. These networks have demonstrated best-in-class performance on all properties in the QM9 computational dataset, which enumerates 134,000 molecules with nine or fewer heavy atoms<sup>14</sup>. Further modifications of the MPNN framework have demonstrated even higher accuracies<sup>15-17</sup>. However, Gilmer *et al.* noted that optimized, equilibrium 3D molecular geometries were required to achieve optimal performance<sup>13</sup>. Since obtaining minimum-energy atomic coordinates is a numerically intensive task, this requirement is limiting for applications in high-throughput chemical screening. Additionally, passing messages between each pair of atoms scales poorly as molecule size increases and is likely infeasible for polymer applications.

While effective, deep learning requires large amounts of data in order to learn appropriate feature representations<sup>18</sup>. However, many applications of deep learning have benefited from *transfer learning*, where weights from a neural network trained on a large dataset are used to initialize weights for a related task with limited data<sup>19</sup>. In this way, the model’s ability to extract useful features from inputs - learned from the larger dataset - is transferred to the new regression task, improving predictive accuracy with fewer training samples. In the molecular space, previous studies have shown that models are able to successfully predict molecules outside their training set<sup>20</sup>, improve their predictive accuracy with additional training on molecules from a different distribution than the prediction target<sup>21</sup>, and estimate non-equilibrium atomic energies at a higher level of theory by pretraining networks on lower-level calculations<sup>22</sup>.

In this study, we apply a MPNN to a recently developed computational dataset of 91,000 optoelectronic calculations for organic photovoltaic (OPV) applications<sup>3</sup>. The dataset consists of both organic polymer candidates, as well as soluble small molecules for solution-processable OPV devices<sup>23,24</sup>. For OPV applications, single-molecule electronic properties play a role in determining overall device efficiency<sup>25-27</sup>, and the search space of molecular structures is sufficiently large that experimental exploration is impractical. We therefore design a ML pipeline to predict optoelectronic properties (*e.g.* HOMO, LUMO, optical excitation energy) directly from a molecule’s connectivity (encoded via SMILES string), without any optimization of molecular structure. We demonstrate that for large molecules, MPNNs trained without explicit spatial information are capable of approaching the estimated optimal error. Moreover, we show that that pre-trained models on one DFT functional are able to improve performance on an alternative DFT functional for limited training data, even when the two target properties are poorly correlated. This successful demonstration of transfer learning in high-throughput materials design suggests that deep learning may be able to leverage success on large-scale computational datasets to improve accuracy on prediction targets involving experimental data or more numerically intensive property simulations.

# Methods

## Dataset preparation

The OPV database<sup>3</sup> consists of calculations performed with a variety of DFT functionals and basis sets (denoted functional/basis below) using the Gaussian 09 electronic structure package with default settings<sup>28</sup>. A detailed description of the molecular structures in the database is left to another publication, however, the structures consist of combinations of building blocks that largely consist of single and multi-ring heterocycles commonly found in OPV applications<sup>2,25,26</sup>. Of these, two datasets were constructed from the two functions with the greatest number of calculations, B3LYP/6-31g(d) and CAM-B3LYP/6-31g. Each dataset consists of monomer or solution-processable small-molecule structures, associated DFT-calculated optoelectronic properties, and, where applicable, corresponding extrapolated polymer properties<sup>29</sup>. The specific electronic properties we predict are: highest occupied molecular orbital (HOMO); lowest unoccupied molecular orbital (LUMO); first excitation energy, calculated with time-dependent DFT (gap); spectral overlap (integrated overlap between the optical absorption spectrum of a dimer and the AM1.5 solar spectrum); optical LUMO (sum of HOMO and gap). Molecular structures were encoded using SMILES strings and did not contain optimized 3D coordinates. The primary B3LYP/6-31g(d) dataset consists of approximately 91,000 molecules with unique SMILES strings, approximately 54,000 of which contain polymer properties. Of these 54,000 with polymer properties, 5,000 were randomly selected for each of the validation and test sets. Transfer learning was examined with a secondary dataset consisting of results from the CAM-B3LYP/6-31g functional. This dataset consists of approximately 32,000 unique molecules, 17,000 of which contain polymer results. From the 17,000 with polymer properties, 2,000 were selected for the validation and test sets. For both datasets, training data were randomly selected from the remainder small molecule and monomer results. Prior to prediction, each property is scaled to have zero median and unit inner quartile range (followed by an inverse transformation after prediction).

Determining an appropriate optimal error rate is an important step in optimizing the hyperparameters of a ML pipeline. In previous studies, target errors were determined based on estimated chemical accuracies for each of the regression tasks<sup>5,13</sup>. However, since many of these parameters are not directly measurable experimentally, we sought to determine a baseline error directly from the data. We therefore used calculation results from conformational isomers: molecules with identical connectivity but different 3D structure. Due to the size of the considered molecules, energy minimization routines can often converge to different lowest-energy states, with slightly altered optoelectronic properties. Since our model only considers atomic connectivity, it cannot distinguish between conformational isomers and predictions for molecules with identical SMILES<sup>30</sup> strings will yield identical predictions. By iterating over all pairs of conformers in the dataset, we calculate a root mean squared error (RMSE) to establish a representative lower limit for predictive accuracy for a model that does not consider 3D atom positions. These optimal errors are presented in Table 1.

## Message Passing Architecture

The molecules considered in this study and used as building blocks for OPV polymers are relatively large, with a maximum size of approximately 200 atoms and bonds (including explicit hydrogens). Inputs to the neural network are generated from the molecules’ SMILES strings, and consists of discrete node types, edge types, and connectivity matrix. Atoms are categorized into discrete types based on their atomic symbol, degree of bonding, and whether or not they are present in an aromatic ring. Bonds are similarly categorized into discrete types based on their type (single, double, triple, or aromatic), conjugation, presence in a ring, and the atom symbols of the two participating atoms.

A schematic of the neural network is shown in Figure 1. The *message passing* step was implemented using the matrix multiplication method<sup>13,31</sup>, where messages  $m$  are passed between neighboring atoms,

$$m_v^{t+1} = \sum_{w \in N(v)} A_{e_{vw}} h_w^t$$

where  $v$  is the node index,  $N(v)$  are the neighboring nodes,  $e_{vw}$  is the bond type,  $h_v^t$  is the feature vector for node  $v$  at step  $t$ , and  $A_{e_{vw}}$  is a learned weight matrix for each bond type.

The *update* step was implemented as a gated recurrent unit block<sup>13</sup>,

$$h_v^{t+1} = \text{GRU}(h_v^t, m_v^{t+1}).$$

Initial atom embeddings,  $h_v^0$ , are initialized randomly for each atom class and learned as additional model parameters. The dimension of the atom state was chosen to be 128, with  $M = 3$  message-passing layers. The readout function used was similar to the one used by Duvenaud and coworkers<sup>12</sup>, but uses only the final hidden state of the recurrent atom unit to generate a whole-graph feature vector  $\hat{y}$ :

$$\hat{y} = \sum_{v \in G} \sigma(Wh_v^M),$$

where  $W$  is a learned weight matrix. The dimension of  $\hat{y}$  was chosen to be 1024. This summed fingerprint is then passed through a series of two fully connected layers with batch normalization and ReLU activation functions (dimensions 512 and 256, respectively), before being passed to an output layer corresponding to each property prediction.

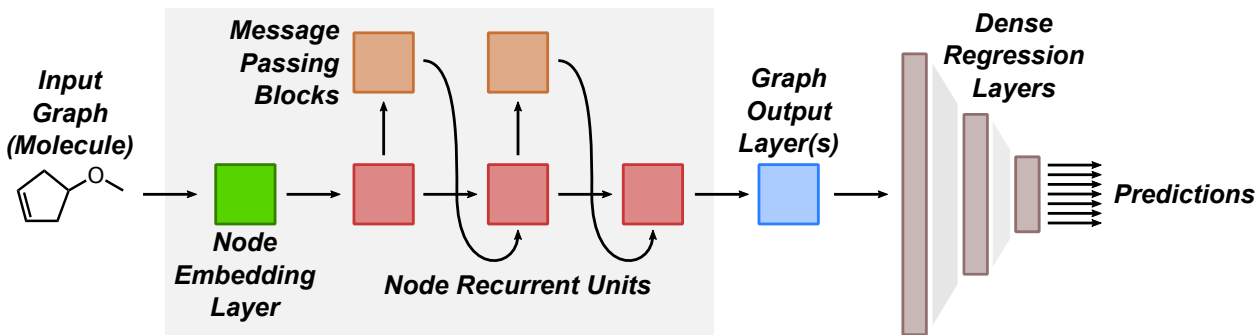


**Figure 1: Schematic of the message passing framework.** Input molecules are labelled according to their atom and bond types. Atom embedding layers are used to initialize the weights of the message passing layers. Molecule-level feature vectors are generated through an output layer which pools all atoms through summation, which is then passed to a series of dense layers to generate a final prediction.

## Results

### Prediction performance on B3LYP/6-31g(d) results

Three separate training strategies were employed to predict the B3LYP/6-31g(d) dataset. First, a separate model was trained for each property (Table 1, “multi-task”). These models were capable of closely matching DFT results, within 31% of the variance expected from differences between conformer results. This result demonstrates the feasibility of high-throughput screening, since accuracies near the irreducible error rate can be generated at ML speed from only a SMILES representation. For speed and transferability, however, a single multi-target model that includes as much chemical knowledge as possible would be preferred. We therefore trained a single neural network to simultaneously predict all eight regression tasks. This multi-task model is close to the performance of the single-task models and exceeds single-task performance on five out of the eight properties (Table 1, “multi-task”). Since the main goal of this method is to predict extrapolated polymer properties, dataset entries corresponding to terminated small-molecule OPV candidates (*i.e.*, those intended for solution-processed devices) were excluded from the training set. However, additional chemical information can be included in the model by augmenting the training data with monomer-level results

from small-molecule calculations. The resulting model has similar performance (on an identical test set) to the model trained without small-molecule results, showing superior performance in five out of eight properties (Table 1, "multi-task, with small molecules"). A parity plot of validation and test set predictions for this model is shown in Figure 3. These results demonstrate that a single model can predict all eight optoelectronic properties at once without a reduction in accuracy.

**Table 1:** Test set prediction errors for models trained on B3LYP/6-31g(d) results. All results are scaled to the RMSE between pairs of conformational isomers (first column) as a baseline optimal error rate. Bold values indicate the model with the lowest error.

B3LYP/6-31g(d)	<i>conformer</i> RMSE	single-task	multi-task	multi-task, with small molecules
gap	0.05 eV	<b>0.90</b>	1.03	0.98
HOMO	0.036 eV	<b>1.05</b>	1.19	1.11
LUMO	0.043 eV	<b>0.89</b>	0.98	0.93
spectral overlap	160 W/mol	1.31	<b>1.28</b>	1.33
Polymer HOMO	0.059 eV	1.28	1.24	<b>1.24</b>
Polymer LUMO	0.067 eV	1.06	<b>1.03</b>	1.05
Polymer gap	0.075 eV	1.27	1.21	<b>1.19</b>
Polymer optical LUMO	0.064 eV	1.09	<b>1.02</b>	1.04

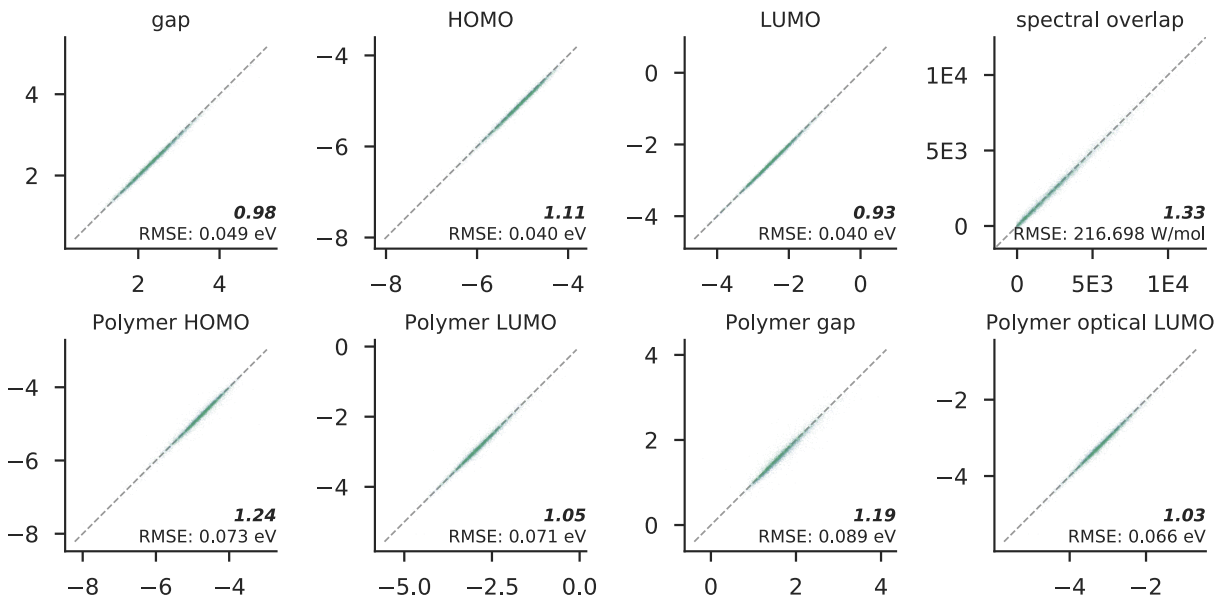


**Figure 2:** Parity plot of out-of-sample ML predictions from the multi-task model augmented with small molecule results. Numbers in bold represent the RMSE divided by the optimal error as determined by conformer results. Test set predictions are plotted in green, while validation set molecules are plotted in blue.

We next explored the effect of training set size on prediction accuracy. Repeated optimizations of the multi-task model were performed with subsampled training data (including small molecules), with the validation set, test set, and model architecture held constant across all experiments. As expected, additional training data causes out-of-sample predictive performance to improve, shown in Figure 3A. At the largest training set sizes, the model’s accuracy asymptotically approaches the optimal error rate.

## Transfer learning to an alternate DFT functional

Finally, we examined whether the molecular representations learned from the large-scale B3LYP/6-31g(d) dataset improved predictive performance on a related regression task. A second, smaller dataset of polymer band gap values calculated using the CAM-B3LYP/6-31g functional was used as a benchmark task. Two single-target models trained on B3LYP/6-31g(d) data were used to initialize the weights for a new single-target prediction model: a model for the same parameter calculated via B3LYP/6-31g(d), and, as a more difficult example, a model for the monomer band gap. The correlation coefficients between the CAM-B3LYP polymer band gap and B3LYP polymer and monomer band gaps were 0.93 and 0.48, respectively, for molecules present in both the CAM-B3LYP/6-31g and B3LYP/6-31g(d) datasets Figure 3C.

Test and validation sets of 2,000 polymer species were reserved, and the remaining training data was sub-divided into training sets of increasing size. All transfer learning strategies were compared against a reference model with random weight initialization for all layers (i.e., no transfer learning). The results of all model predictions on the test set are shown in Figure 3B. For each model, performance is compared an estimated upper error bound. For the reference model, this was estimated as the RMSE assuming the model always predicted the mean value of the test set. For the models with transferred weights, a baseline model was assumed that would predict first the value of the pretrained B3LYP/6-31g(d) property, then transform that value via a linear model to best match the CAM-B3LYP polymer band gap. The RMSEs for these two hypothetical models were calculated as 0.36 eV and 0.15 eV for B3LYP/6-31g(d) monomer band gap and polymer band gap, respectively. For models with weight transfer, performance superior to these estimated upper error limits indicates that the model has learned to extract and process salient features of the molecules related to the new prediction target - rather than simply recalling and rescaling the previously learned prediction target.

For very small training set sizes (on the order of 200 molecules), models performed near the estimated upper error bound with the notable exception of model with weakly correlated transferred weights, which had a substantially lower test set error than expected. This application demonstrates that pretraining models on even slightly related prediction targets could likely improve out-of-sample prediction accuracy when the available data is limited. As the available training data is increased, both models with transferred weights demonstrate a concomitant decrease in their test set error below their estimated upper bound error. In particular, the model with weights transferred from the strongly correlated task shows superior performance at all training set sizes, requiring nearly an order of magnitude less data to reach RMSE values of 0.1 eV. At the largest training set sizes all three models approach the optimal error rate estimated through conformers with duplicated SMILES strings, indicating that knowledge encapsulated in transferred weights is eventually replaced with knowledge gained through the new training data.

## Conclusions

We have shown that a deep neural network pretrained on one DFT functional was able to improve predictive performance on a related DFT functional, especially in the case of limited data. This performance improvement is dependent on the correlation between tasks, but even weights transferred from a network trained on a weakly correlated task were able to improve accuracy. These results help to confirm the immense value of machine learning approaches in scientific domains both to increase the fidelity of DFT simulations and to augment them, allowing for high throughput screening and guided search. Future work will therefore explore the ability of pretrained neural networks to improve prediction accuracy on experimental data and other important targets with limited available data. Additionally, we demonstrate that prediction errors near experimental error (and approximately equal to the errors expected from complex molecular structure optimization) can be reached with ML algorithms trained without optimized 3D geometry. This is a key finding, as determining stable configurations of molecules in a high-throughput fashion would otherwise be the dominant computational cost in applying MPNNs for high-throughput screening.

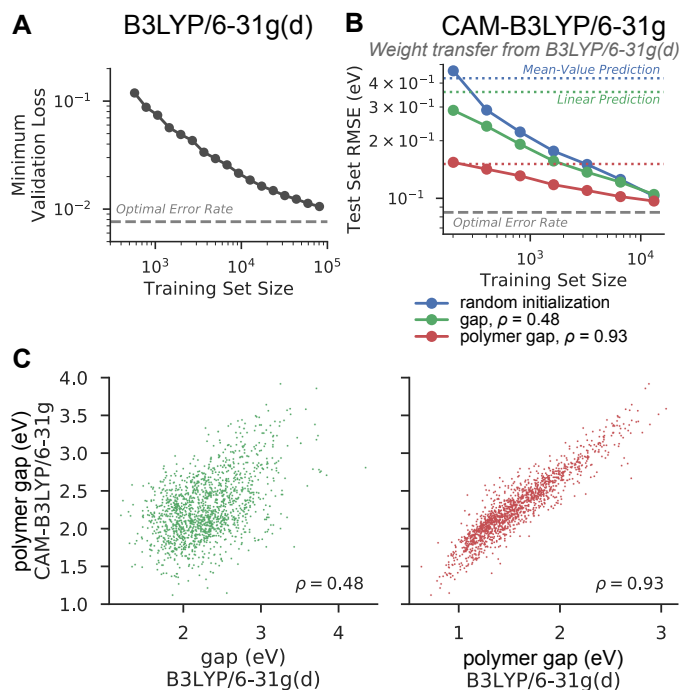


**Figure 3: Effect of training set size on predictive performance** (A) Training on B3LYP/6-31g(d). Models gradually approach the optimal error rate as training set size increases. (B) Transfer learning to predict polymer band gap calculated with CAM-B3LYP/6-31g. For each model, performance is compared to both the optimal error rate and an estimated upper error bound based on a simple linear model (dotted lines). (C) Plot of CAM-B3LYP polymer band gap versus the single-target properties used for pretraining: monomer band gap (left) and polymer band gap (right). Points represent molecules with results calculated via both functionals.

ML approaches may also be useful in other applications in optimizing polymer properties from a wide range of possible monomers. Biomass feedstocks in particular offer a wide range of potential building blocks for performance-advantaged materials, but experimental exploration of the each resulting polymer's properties is time-consuming and costly. Transfer learning from related, computational experiments may therefore offer a method for screening materials for specific applications.

## Computational Methods

### Software

Message passing operations were implemented using Keras and Tensorflow. Scikit-learn was used to scale the prediction targets, and rdkit was used to encode the atoms and bonds as integer classes.

### Hyperparameter optimization

Model sizes (atom vector dimension, molecule vector dimension, number and size of dense layers) were increased until training errors fell below the target optimal error rate while the model still fitting on single GPU (Tesla K80) with a batch size of 100. Models were optimized using the ADAM optimizer. Learning rates were varied between 1E-2 and 1E-5, with 1E-3 yielding the best result. Explicit learning rate decay was also noticed to improve optimization, a decay value of 2E-6 each epoch was used. Models were trained for 500 epochs. Methods for explicit regularization, including dropout and  $l_2$  schemes were tried, but did not decrease the validation loss. All models (including refitting weights during transfer learning) used early stopping by evaluating the validation loss every 10 epochs and using the model which yielded the lowest validation loss.

## Acknowledgements

This work was supported by the U.S. Department of Energy under Contract No. DE-AC36-08GO28308 with Alliance for Sustainable Energy, LLC, the Manager and Operator of the National Renewable Energy Laboratory. Funding was provided by U.S. Department of Energy, Office of Bioenergy Technologies (DOE-BETO) under the Performance Advantaged Bioproducts working group. The views and opinions of the authors expressed herein do not necessarily state or reflect those of the United States Government or any agency thereof. Neither the United States Government nor any agency thereof, nor any of their employees, makes any warranty, expressed or implied, or assumes any legal liability or responsibility for the accuracy, completeness, or usefulness of any information, apparatus, product, or process disclosed, or represents that its use would not infringe privately owned rights.



## References

- (1) Jain, A.; Ong, S. P.; Hautier, G.; Chen, W.; Richards, W. D.; Dacek, S.; Cholia, S.; Gunter, D.; Skinner, D.; Ceder, G.; et al. Commentary: The Materials Project: A Materials Genome Approach to Accelerating Materials Innovation. *APL Mater* **2013**, *1* (1), 011002.
- (2) Lopez, S. A.; Pyzer-Knapp, E. O.; Simm, G. N.; Lutzow, T.; Li, K.; Seress, L. R.; Hachmann, J.; Aspuru-Guzik, A. The Harvard Organic Photovoltaic Dataset. *Sci Data* **2016**, *3*, 160086.
- (3) Larsen, R.; Olson, D.; Kopidakis, N.; Owczarczyk, Z.; Hammond, S.; Graf, P.; Kemper, T.; Sides, S.; Munch, K.; Evenson, D.; et al. Computational Database for Active Layer Materials for Organic Photovoltaic Solar Cells.
- (4) Ruddigkeit, L.; Deursen, R. van; Blum, L. C.; Reymond, J.-L. Enumeration of 166 Billion Organic Small Molecules in the Chemical Universe Database Gdb-17. *J Chem Inf Model* **2012**, *52* (11), 2864–2875.
- (5) Faber, F. A.; Hutchison, L.; Huang, B.; Gilmer, J.; Schoenholz, S. S.; Dahl, G. E.; Vinyals, O.; Kearnes, S.; Riley, P. F.; von Lilienfeld, O. A. Prediction Errors of Molecular Machine Learning Models Lower Than Hybrid DFT Error. *J Chem Theory Comput* **2017**, *13* (11), 5255–5264.
- (6) Katritzky, A. R.; Kuanar, M.; Slavov, S.; Hall, C. D.; Karelson, M.; Kahn, I.; Dobchev, D. A. Quantitative Correlation of Physical and Chemical Properties with Chemical Structure: Utility for Prediction. *Chem Rev* **2010**, *110* (10), 5714–5789.
- (7) Brown, W. M.; Martin, S.; Rintoul, M. D.; Faulon, J.-L. Designing Novel Polymers with Targeted Properties Using the Signature Molecular Descriptor. *J Chem Inf Model* **2006**, *46* (2), 826–835.
- (8) Maranas, C. D. Optimal Computer-Aided Molecular Design: a Polymer Design Case Study. *Ind Eng Chem Res* **1996**, *35* (10), 3403–3414.
- (9) Pilania, G.; Wang, C.; Jiang, X.; Rajasekaran, S.; Ramprasad, R. Accelerating Materials Property Predictions Using Machine Learning. *Sci Rep* **2013**, *3* (1).
- (10) St. John, P. C.; Kairys, P.; Das, D. D.; McEnally, C. S.; Pfefferle, L. D.; Robichaud, D. J.; Nimlos, M. R.; Zigler, B. T.; McCormick, R. L.; Foust, T. D.; et al. A Quantitative Model for the Prediction of Sooting Tendency from Molecular Structure. *Energy Fuels* **2017**, *31* (9), 9983–9990.
- (11) Das, D. D.; John, P. C. S.; McEnally, C. S.; Kim, S.; Pfefferle, L. D. Measuring and Predicting Sooting Tendencies of Oxygenates, Alkanes, Alkenes, Cycloalkanes, and Aromatics on a Unified Scale. *Combust Flame* **2018**, *190*, 349–364.
- (12) Duvenaud, D. K.; Maclaurin, D.; Iparraguirre, J.; Bombarell, R.; Hirzel, T.; Aspuru-Guzik, A.; Adams, R. P. Convolutional Networks on Graphs for Learning Molecular Fingerprints. *Adv Neural Inf Process Syst* **2015**, *28*, 2224–2232.
- (13) Gilmer, J.; Schoenholz, S. S.; Riley, P. F.; Vinyals, O.; Dahl, G. E. Neural Message Passing for Quantum Chemistry. *Int Conf Machine Learning* **2017**.
- (14) Ramakrishnan, R.; Dral, P. O.; Rupp, M.; von Lilienfeld, O. A. Quantum Chemistry Structures and Properties of 134 Kilo Molecules. *Sci Data* **2014**, *1*.
- (15) Schütt, K.; Kindermans, P.-J.; Saucedo Felix, H. E.; Chmiela, S.; Tkatchenko, A.; Müller, K.-R. SchNet: A Continuous-Filter Convolutional Neural Network for Modeling Quantum Interactions. *Adv Neural Inf Process Syst* **2017**, *30*, 991–1001.
- (16) Schütt, K. T.; Saucedo, H. E.; Kindermans, P.-J.; Tkatchenko, A.; Müller, K.-R. SchNet – a Deep Learning Architecture for Molecules and Materials. *J Chem Phys* **2018**, *148* (24), 241722.
- (17) Jørgensen, P. B.; Jacobsen, K. W.; Schmidt, M. N. Neural Message Passing with Edge Updates for Predicting Properties of Molecules and Materials. *arXiv* **2018**, arXiv:1806.03146.
- (18) LeCun, Y.; Bengio, Y.; Hinton, G. Deep Learning. *Nature* **2015**, *521* (7553), 436–444.

- (19) Yosinski, J.; Clune, J.; Bengio, Y.; Lipson, H. How Transferable Are Features in Deep Neural Networks? *Adv Neural Inf Process Syst* **2014**, *27*, 3320–3328.
- (20) Smith, J. S.; Isayev, O.; Roitberg, A. E. ANI-1: An Extensible Neural Network Potential with DFT Accuracy at Force Field Computational Cost. *Chem Sci* **2017**, *8* (4), 3192–3203.
- (21) Schütt, K. T.; Arbabzadah, F.; Chmiela, S.; Müller, K. R.; Tkatchenko, A. Quantum-Chemical Insights from Deep Tensor Neural Networks. *Nat Commun* **2017**, *8*, 13890.
- (22) Smith, J. S.; Nebgen, B. T.; Zubatyuk, R.; Lubbers, N.; Devereux, C.; Barros, K.; Tretiak, S.; Isayev, O.; Roitberg, A. Outsmarting Quantum Chemistry Through Transfer Learning. *ChemRxiv* **2018**.
- (23) Lloyd, M. T.; Anthony, J. E.; Malliaras, G. G. Photovoltaics from Soluble Small Molecules. *Mater Today* **2007**, *10* (11), 34–41.
- (24) Poll, T. S. van der; Love, J. A.; Nguyen, T.-Q.; Bazan, G. C. Non-Basic High-Performance Molecules for Solution-Processed Organic Solar Cells. *Adv Mater* **2012**, *24* (27), 3646–3649.
- (25) Oosterhout, S. D.; Kopidakis, N.; Owczarczyk, Z. R.; Braunecker, W. A.; Larsen, R. E.; Ratcliff, E. L.; Olson, D. C. Integrating Theory, Synthesis, Spectroscopy and Device Efficiency to Design and Characterize Donor Materials for Organic Photovoltaics: A Case Study Including 12 Donors. *J Mat Chem A* **2015**, *3* (18), 9777–9788.
- (26) Scharber, M.; Mühlbacher, D.; Koppe, M.; Denk, P.; Waldauf, C.; Heeger, A.; Brabec, C. Design Rules for Donors in Bulk-Heterojunction Solar Cells—Towards 10% Energy-Conversion Efficiency. *Adv Mater* **2006**, *18* (6), 789–794.
- (27) Li, N.; McCulloch, I.; Brabec, C. J. Analyzing the Efficiency, Stability and Cost Potential for Fullerene-Free Organic Photovoltaics in One Figure of Merit. *Energy Environ Sci* **2018**, *11* (6), 1355–1361.
- (28) Frisch, M. J.; Trucks, G. W.; Schlegel, H. B.; Scuseria, G. E.; Robb, M. A.; Cheeseman, J. R.; Scalmani, G.; Barone, V.; Mennucci, B.; Petersson, G. A.; et al. Gaussian 09 Revision D.1.
- (29) Larsen, R. E. Simple Extrapolation Method to Predict the Electronic Structure of Conjugated Polymers from Calculations on Oligomers. *J Phys Chem C* **2016**, *120* (18), 9650–9660.
- (30) Weininger, D. SMILES, a Chemical Language and Information System. 1. Introduction to Methodology and Encoding Rules. *J Chem Inf Model* **1988**, *28* (1), 31–36.
- (31) Li, Y.; Tarlow, D.; Brockschmidt, M.; Zemel, R. Gated Graph Sequence Neural Networks. *Int Conf Learn Represent* **2016**.